



OPEN PGE2 regulates ferroptosis and osteogenesis of MC3T3-E1 cells via NOS2

Mengling Sun¹, Yingying Yang^{1,2}, Liying Pang¹, Jiaying Yang¹, You Li³, Chen Lin^{4,5}✉ & Linkun Zhang^{4,5}✉

Prostaglandin E2 (PGE2) is a key inflammatory mediator in orthodontic tooth movement, yet its precise role in regulating osteogenesis remains unclear. This study investigated the mechanism by which PGE2 influences ferroptosis and osteogenesis in MC3T3-E1 cells, focusing on nitric oxide synthase 2 (NOS2). Bioinformatic analysis identified NOS2 as a core ferroptosis-related gene after orthodontic force loading. 100 ng/mL PGE2 induced sterile inflammation and ferroptosis as evidenced by upregulated expressions of IL-6, NOS2, and ACSL4 while downregulated expressions of GPX4, FTH1 detected by RT-qPCR and western blot, alongside promoted reactive oxygen species and malondialdehyde production detected by flow cytometry. Meanwhile, PGE2 inhibited osteogenesis characterized by downregulated expressions of osteogenic markers RUNX2, Osterix, OPN, OCN and diminished ALP activity and mineralization level detected by RT-qPCR, western blot, ALP staining, ARS staining, ALP activity detection and Ca²⁺ level assessment. Effects following PGE2 treatment were rescued by the ferroptosis inhibitor Ferrostatin-1. Crucially, NOS2 knockdown mitigated PGE2-induced ferroptosis and osteogenic suppression, whereas NOS2 overexpression exacerbated them. Furthermore, NOS2 overexpression alone sufficed to promote ferroptosis and inhibit osteogenesis absent inflammation. In conclusion, PGE2 induces sterile inflammation, it also triggers ferroptosis and inhibits osteogenesis via NOS2, revealing a novel molecular axis in bone remodeling during orthodontic treatment.

Keywords PGE2, NOS2, Sterile inflammation, Ferroptosis, Osteogenesis

Orthodontic treatment is crucial for improving facial aesthetics and stomatognathic function. However, the prolonged treatment duration not only increases the risk of oral diseases such as dental caries¹ but also poses challenges in maintaining stable treatment outcomes. Therefore, developing clinically safe and efficient strategies to accelerate orthodontic tooth movement (OTM) is imperative, which necessitates a deeper understanding of its underlying biological mechanisms. The foundation of OTM lies in the remodeling of alveolar bone, a process involving a series of complex cellular biological events within the periodontal microenvironment². Among these, sterile inflammation³ and ferroptosis⁴, a newly recognized form of regulated cell death, have emerged as significant factors influencing the bone remodeling process. Nevertheless, the specific molecular pathways through which inflammatory signals lead to cellular dysfunction and ultimately affect osteogenic differentiation remain incompletely understood.

In the context of OTM, prostaglandin E2 (PGE2) is a key inflammatory mediator that can be locally induced in periodontal tissues by mechanical orthodontic force⁵. Elevated levels of PGE2 in the periodontal ligament, alveolar bone, and gingival crevicular fluid following force application have been observed, and its functional importance is underscored by the fact that OTM can be slowed by inhibitors of prostaglandin synthesis^{6,7}. Although the role of PGE2 in promoting osteoclastogenesis and bone resorption on the pressure side is well-established, its specific signaling mechanisms in osteoblasts—the cells responsible for bone formation on the tension side—remain unclear, representing a critical knowledge gap. Our previous study indicated that PGE2 could indirectly inhibit osteogenic differentiation via exosomes⁸, hinting at its complex regulatory role.

¹School of Clinical Stomatology, Tianjin Medical University, Tianjin 300070, China. ²Fuzhou Second General Hospital, Fuzhou 350007, China. ³Department of Orthodontics, Chengfei Dental, Guangzhou 510000, China.

⁴Department of Orthodontics, School of Medicine, Tianjin Stomatological Hospital, Nankai University, Tianjin 300041, China. ⁵Tianjin Key Laboratory of Oral and Maxillofacial Function Reconstruction, Tianjin 300070, China.

✉email: linchen2119@qq.com; linkunzhang@nankai.edu.cn

Notably, PGE2 has also been implicated in regulating ferroptosis, an iron-dependent form of cell death driven by the lethal accumulation of lipid peroxides⁹. Ferroptosis has been demonstrated to directly inhibit the osteogenic differentiation and mineralization capacity of osteoblasts, thereby negatively impacting bone remodeling under mechanical stress^{10,11}. This positions ferroptosis as a potential downstream executor of inflammatory signals that may lead to osteoblast dysfunction. However, PGE2 and has different effects on the occurrence and progression of ferroptosis under various conditions^{12–14}. The precise mechanism by which PGE2, as an upstream inflammatory signal, triggers ferroptosis in osteoblasts remains to be elucidated.

We hypothesized that nitric oxide synthase 2 (NOS2) could serve as a potential central mediator bridging this gap. NOS2 is a key inflammatory factor induced under various stresses^{15,16}. In osteoblastic cell lines, a close and complex interaction exists between the PGE2 and NOS2 signaling pathways¹⁷. Also, it's observed that the secretion of PGE2 and the expression of NOS2 of mouse osteocytes were increased under mechanical strain¹⁸. In the context of OTM, studies have observed the upregulation of NOS2 in alveolar bone under orthodontic force and linked it to inflammation-induced bone resorption^{19,20}. Furthermore, preliminary gene expression data from our previous rat OTM model also indicated upregulated NOS2 expression in alveolar bone following force application. More importantly, evidence suggests that NOS2 and its downstream product, nitric oxide (NO), can participate in the ferroptosis process under certain conditions by influencing cellular iron metabolism and amplifying oxidative stress²¹, and that inhibiting NOS2 can significantly alleviate ferroptosis in an inflammatory environment²². Although PGE2, ferroptosis, and NOS2 have all been confirmed to participate in bone remodeling, how these three components form a direct regulatory network in osteoblasts has not been investigated.

This study aims to validate this “PGE2-NOS2-ferroptosis” axis using the MC3T3-E1 osteoblastic cell line. Our findings provided a novel molecular perspective on bone remodeling during OTM and identify potential therapeutic targets for enhancing orthodontic treatment efficiency.

Materials and methods

Screening of core genes associated with OTM and ferroptosis

Gene expression profiles before and after orthodontic force application in a periodontally healthy rat OTM model were obtained by whole transcript expression arrays in our prior research, intersected with the ferroptosis-related genes obtained from the FerrDb database (<http://www.zhounan.org/ferrdb>) to identify overlapping genes. These differential genes were imported into the STRING database (<https://cn.string-db.org/>) for PPI network construction, and the results of core genes were visualized using Cytoscape (<https://cytoscape.org/>).

Cell culture

The MC3T3-E1 cell line was obtained from Tianjin Key Laboratory of Oral and Maxillofacial Function Reconstruction (Tianjin, China) and was cultured in complete medium consisting of α -MEM supplemented with 10% fetal bovine serum and 1% penicillin-streptomycin in an environment of FiO₂ (21%), 37 °C, and 5% CO₂. PGE2-containing medium was prepared with different concentrations of PGE2, and the cells were cultured for 24 h. Fer-1 containing medium was prepared with ferrostatin-1, and the cells were pretreated for 2 h before the medium was replaced with PGE2-containing medium. Osteogenic differentiation induction medium was prepared with 50 mg/mL ascorbic acid, 10 mM β -glycerol phosphate disodium salt, 10 mM dexamethasone, and complete medium. The cells were cultured for 14 days to induce osteogenic differentiation. The medium was replaced every 3 days. Cells were collected after relative culture for further detection.

Cell proliferation assay: CCK-8

The cells were inoculated into 96-well plates at a density of 1000 cells per well and cultured in PGE2-containing medium at concentrations of 0, 10 ng/mL, 100 ng/mL, 1 μ g/mL, or 10 μ g/mL for 24 h. On days 1, 3, 5, and 7 posttreatment, the prepared CCK-8 assay reagent was added to each well. The optical density (OD) was detected at 450 nm. The cell viability rate was calculated via the following formula: cell viability rate (%) = [(OD value of experimental well – OD value of blank well)/(OD value of control well - OD value of blank well)] \times 100%.

Real time quantitative PCR (RT-qPCR)

The cells were inoculated into 6-well plates and cultured with different media according to the experimental groups for the required duration. After the cells were collected, total RNA was extracted via the Steady Pure RNA Extraction Kit (AGbio, China). The RNA concentration was measured with a spectrophotometer (Bio-Rad Laboratories, USA). Complementary DNA (cDNA) was synthesized via an RNA reverse transcription kit (AGbio, China). The resulting cDNA was analysed via RT-qPCR using the SYBR Green Pro Taq HS Premix qPCR Kit (AGbio, China). The reactions were performed in a total volume of 20 μ L, consisting of 10 μ L of 2 \times SYBR Green Pro Taq HS Premix™, 0.4 μ L of PCR forward primer (10 μ M), 0.4 μ L of PCR reverse primer (10 μ M), 7.2 μ L of RNase-free dH₂O, and 2 μ L of cDNA (50 ng/ μ L). PCR was conducted with a real-time fluorescent quantitative PCR instrument (Bio-Rad Laboratories, USA). The reaction conditions were as follows: initial denaturation at 95 °C for 30 s, followed by 40 cycles of denaturation at 95 °C for 5 s and extension at 60 °C for 30 s. The mRNA levels of the target genes were determined via the cycle threshold method (2^{− $\Delta\Delta$ Ct}), with GAPDH serving as the internal control. The primers sequences were listed in Table 1.

Western blot

The solution was prepared for protein extraction from cells by mixing phenylmethylsulfonyl fluoride (PMSF) with Cell Complete Lysis Buffer for Western blotting and IP (Beyotime, China) at a ratio of 1:100 and was quantified via a BCA protein assay kit (Beyotime, China). The proteins were separated in Gly-Tris, 4–20% BeyoGel™ Plus PAGE Precast Gels (Beyotime, China), transferred to polyvinylidene fluoride (PVDF) membranes, blocked

Gene	Sequence
ACSL4	Forward: 5-TGAACGTATCCCTGGACTAGG-3 Reverse: 5-TCAGACAGTGTAAAGGGGTGAA-3
FTH1	Forward: 5-CCGAGATGATGTGGCTCTGAA-3 Reverse: 5-GTAGCCAGTTTGTGCAGTTCC-3
GAPDH	Forward: 5-CAGCAACTCCCCTCTTC-3 Reverse: 5-TGTAGCCGATTTCATTGTC-3
GPX4	Forward: 5-GCCTGGATAAGTACAGGGGT-3 Reverse: 5-CATGCAGATCGACTAGCTGAG-3
IL-6	Forward: 5-CTATACCACTTCACAAGTCGGA-3 Reverse: 5-GAATTGCCATTGCACAACCTTT-3
NOS2	Forward: 5-GGAGTGACGGCAAACATGACT-3 Reverse: 5-TCGATGCACAACCTGGGTGAAC-3
OCN	Forward: 5-GGTGCAGACCTAGCAGACACCA-3 Reverse: 5-AGGTAGCGCCGGAGTCTATTCA-3
OPN	Forward: 5-AGCAAGAACTCTTCCAAGCAA-3 Reverse: 5-GTGAGATTTCGTCAGATTTCATCCG-3
Osterix	Forward: 5-TGAACGTATCCCTGGACTAGG-3 Reverse: 5-TCAGACAGTGTAAAGGGGTGAA-3
RUNX2	Forward: 5-CGTCCTCTCTGCTTGAGGAA-3 Reverse: 5-TTCCCAGGGCTGTTGAGTC-3

Table 1. Primer sequence.

with QuickBlock™ Blocking Buffer (Beyotime, China) for 1.5 h at room temperature, and then probed with the corresponding primary antibodies against GPX4 (ABclonal, USA), FTH1 (ABclonal, USA), ACSL4 (ABclonal, USA), OPN (Abcam, USA), OCN (ABclonal, USA), RUNX2 (Cell Signaling Technology, USA), Osterix (Abcam, USA), and GAPDH (ABclonal, USA) overnight at 4 °C. An ultrasensitive ECL Chemiluminescence Kit (Beyotime, China) was used for protein visualization after incubation with an HRP-conjugated anti-rabbit secondary antibody (Proteintech, China). Due to the similar identical molecular weights of OPN and GAPDH, the PVDF membrane was first incubated with the primary antibody against OPN and then corresponding secondary antibody. The antibodies were stripped off by stripping buffer after visualization. Subsequently, the same PVDF membrane was re-probed with the primary antibody against GAPDH and then corresponding secondary antibody. Images were captured with an Amersham Imager 680 (GE Healthcare Life Sciences, USA). The gray value was quantified with ImageLab 6.0 software.

Detection of the malondialdehyde (MDA) level

Total cellular protein was extracted and the concentration was determined. The samples were prepared according to the instructions of the MDA assay kit (Beyotime, China). The absorbance at a wavelength of 532 nm was detected. The MDA concentration was calculated according to the standard curve, and the intracellular MDA level per unit weight of protein was calculated on the basis of the previously determined protein concentration.

ROS level detection

The cells were digested and collected in 1.5 mL sterile centrifuge tubes, resuspended in DCFH-DA solution diluted with α -MEM at a ratio of 1:1000, incubated at 37 °C for 30 min and gently inverted every 5 min during the process. The extra DCFH-DA was removed, and a cell suspension was prepared with phosphate buffered saline (PBS). All the experiments were carried out in the dark. Given that the fluorescence spectra of fluorescein isothiocyanate (FITC) and 2',7'-Dichlorofluorescein (DCF) are very similar, the detection parameters can be set to those of FITC to measure DCF by flow cytometry according to the instrument's instructions. The results were imported into FlowJo 10.8.1 software for analysis.

ALP staining and ALP activity detection

ALP Staining: On day 14 of osteogenic induction, ALP staining was performed. The cells were rinsed with PBS and fixed with 4% paraformaldehyde (PFA) for 15 min. ALP staining solution (Beyotime, China) was prepared according to the protocol and added to 6-well plates. The cells were incubated in the dark for 30 min, rinsed with ultrapure water and imaged under a microscope (Ti-S, Nikon, Japan).

Alkaline Phosphatase Activity Assay (pNPP method): After 14 days of osteogenic induction, cellular proteins were collected and centrifuged at 12,000 rpm and 4 °C for 10 min. The supernatant was collected for detection. A standard working solution with a final concentration of 0.5 mM was prepared by mixing p-nitrophenol (10 mM) with detection buffer at a volume ratio of 1:190 (Beyotime, China). The reaction system was set up according to the instructions and incubated at 37 °C for 20 min. After the reaction was terminated, the absorbance at a wavelength of 405 nm was detected.

ARS staining and Ca²⁺ level detection

Alizarin Red S (ARS) Staining: On day 14 of osteogenic induction, ARS staining was performed. The cell treatment procedure was the same as that for ALP staining. Alizarin Red S staining solution was incubated with

the cells in the dark for 10 min, gently rinsed with ultrapure water, and replaced with an appropriate amount of PFA. The cells were imaged under a microscope (Ti-S, Nikon, Japan).

Ca²⁺ level detection: After alizarin red S staining and image acquisition, 10% cetylpyridinium chloride solution was prepared, added to 6-well plates, and incubated at room temperature in the dark for 30 min. Then, 100 μ L of the solution was added to each well of a 96-well plate, and the absorbance at 562 nm was detected.

Knockdown (KD) and overexpression (OE) of NOS2

Cell culture was carried out following the aforementioned procedures. When the cells reached 70–80% confluence, the transfection mixture was prepared according to the manufacturer's protocol for the Lipo8000™ Transfection Reagent (Beyotime, China). Transfection of Mus-Nos2-shRNA (Keyanyun Biotechnology, China), mouse Nos2 pCDH-CMV-MCS-3*FLAG-EF1a-CopGFP-T2A-Puro-WPRE (Keyanyun Biotechnology, China), and corresponding vectors was then performed to achieve NOS2 knockdown and overexpression.

Statistical analysis

All experimental results are presented as mean \pm standard deviation (SD). Consistency tests were conducted on the data from each group. Data that met the criteria were analysed via one-way analysis of variance (ANOVA) and Fisher's least significant difference (LSD) test. Statistical analysis and chart generation were performed with GraphPad Prism 9.3 software. Differences were considered statistically significant when $P < 0.05$.

Results

NOS2 was a core, ferroptosis-related, differentially expressed gene following orthodontic force application

In the alveolar bone tissue of periodontally healthy rats, 34 intersecting genes were identified from the differentially expressed genes between the orthodontic force-loading group and the control group that were related to ferroptosis (Fig. 1A). These 34 differential genes were imported into the STRING database to construct a visual PPI network (Fig. 1B). Further analysis using Cytoscape identified eight core genes: *IL-6*, *IL-1 β* , *NOS2*, *Cxcl2*, *Ptgs2*, *Hif1 α* , and *Hmox1* (Fig. 1C).

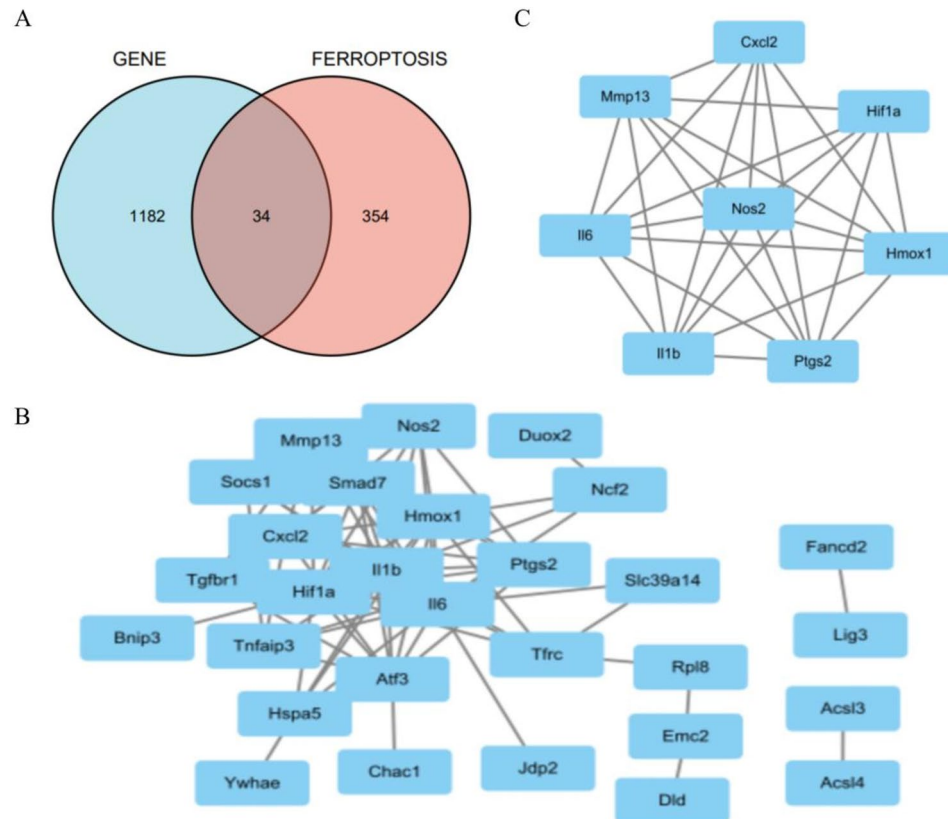


Fig. 1. Differentially expressed gene associated with ferroptosis in periodontally healthy rat after orthodontic force loading. (A) Intersection of differentially expressed genes in rat alveolar bone between orthodontic force-loaded and non-loaded groups with ferroptosis-related genes; (B) PPI network of proteins encoded by the differentially expressed genes; (C) Core genes associated with ferroptosis.

PGE2 promoted the expression of NOS2 and induced sterile inflammation and ferroptosis

To induce a state of sterile inflammation *in vitro*, we firstly confirmed the inflammation inducing effects of PGE2 on MC3T3-E1 cells and sought to determine the optimal effective concentration of PGE2. The proliferation of MC3T3-E1 cells treated with different concentrations of PGE2 was not significantly different (Fig. 2A). Compared to control group, the relative mRNA expression levels of the inflammatory factors *Il-6* and *Nos2* increased in a PGE2 concentration-dependent manner, with statistically significant differences observed at concentrations of 100 ng/mL and above (Fig. 2B,C), indicating successful induction of sterile inflammation in MC3T3-E1 cells. As for ferroptosis inducing effect, the mRNA expression levels of ferroptosis-related markers ferritin heavy polypeptide 1 (*Fth1*) and glutathione peroxidase 4 (*Gpx4*) decreased (Fig. 2E,F), whereas ROS production increased compared to control group, with statistically significant differences observed at PGE2 concentrations of 100 ng/mL and above (Fig. 2G and H). The increases in Acyl-CoA synthetase long-chain family member 4 (*Acs14*) mRNA expression (Fig. 2D) and MDA production (Fig. 2I) were statistically significant only at a PGE2 concentration of 100 ng/mL. Based on results above, we chose 100 ng/mL as the concentration of PGE2 for subsequent experiments.

Fer-1 mitigated the sterile inflammation, ferroptosis and osteogenesis inhibition induced by PGE2

To further verify that whether PGE2 promotes ferroptosis, we selected the well-recognized ferroptosis inhibitor Fer-1 as a reference. Compared to control group, the OD values obtained from the CCK-8 assay tended to decrease with increasing Fer-1 concentration, with statistically significant differences observed at concentrations of 10 μ M and 20 μ M (Fig. 3A). On the basis of these findings, we chose 10 μ M as the concentration of Fer-1 for subsequent experiments. Moreover, there was no statistically significant difference among the PGE2, Fer-1 + PGE2 and control groups (Fig. 3B), indicating that the intervention concentrations applied to the experimental groups had no significant effect on the survival rate of MC3T3-E1 cells. After Fer-1 treatment, the changes in the expression levels of inflammation-related indicators *Il-6*, *Nos2* (Fig. 3C,D) and ferroptosis-related indicators *Acs14*, *Fth1*, *Gpx4* (Fig. 3E–G) induced by PGE2 were significantly reversed. Fer-1 also reduced the promoted production of ROS (Fig. 3H,I) and MDA (Fig. 3J). At the same time, we investigated the impact of PGE2 on the osteogenesis of MC3T3-E1 cells. After PGE2 treatment, the mRNA expressions of runt-related transcription factor 2 (*Runx2*), osteopontin (*Opn*), osteocalcin (*Ocn*), and *Osterix* were significantly downregulated (Fig. 3K–N). Results above indicated that 100 ng/mL PGE2 could simultaneously induce sterile inflammation and ferroptosis as well as inhibited osteogenesis of MC3T3-E1 cells and these effects could be mitigated by Fer-1 at a concentration of 10 μ M.

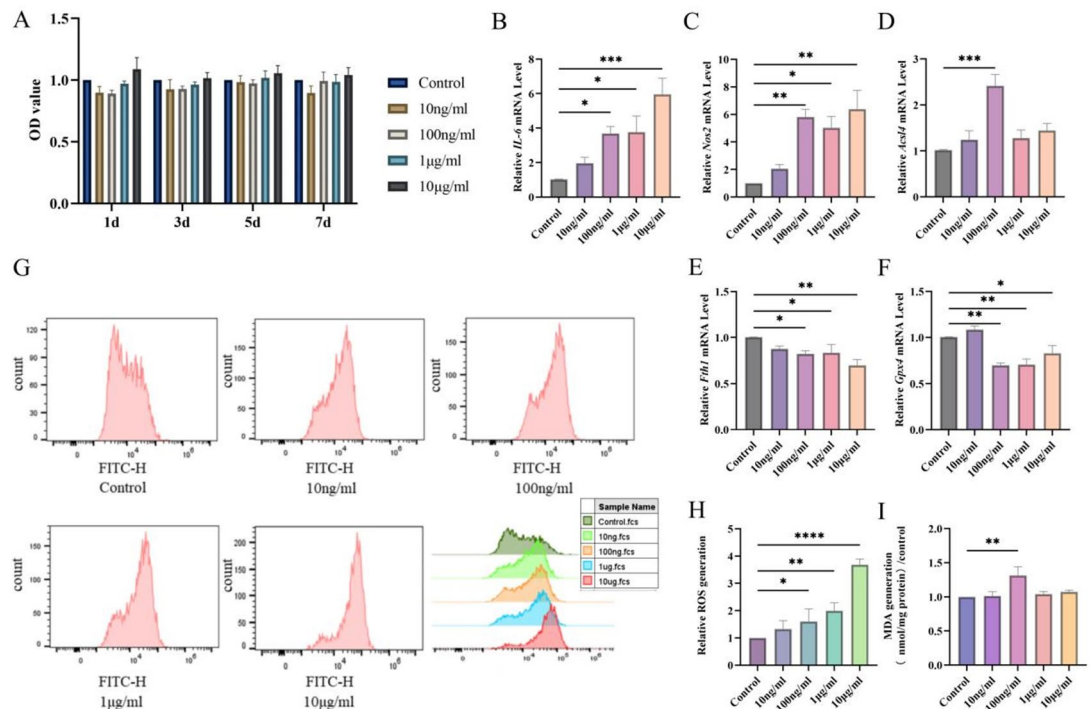


Fig. 2. Optimization of PGE2 concentrations and effects on sterile inflammation and ferroptosis. (A) Cell viability of MC3T3-E1 cells after treatment with varying concentrations of PGE2. (B–F): The mRNA expressions of *IL-6*, *Nos2*, *Acs14*, *Fth1* and *Gpx4* after treatment with varying concentrations of PGE2. (G,H): Relative ROS levels after treatment with varying concentrations of PGE2 assessed by flow cytometry. (I) Relative MDA levels after treatment with varying concentrations of PGE2. * $P < 0.05$, ** $P < 0.01$, *** $P < 0.001$, **** $P < 0.0001$.

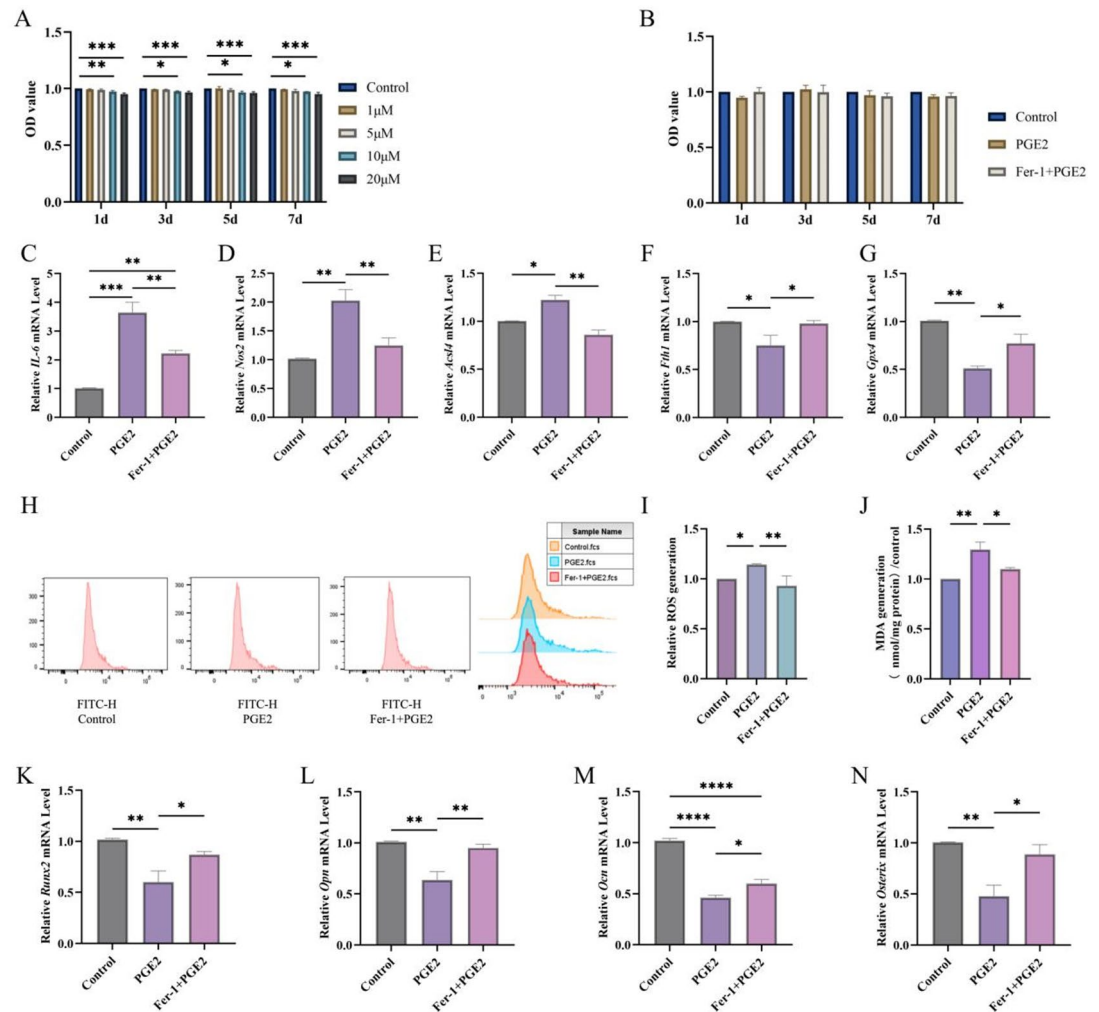


Fig. 3. Optimization of Fer-1 concentrations and its antagonistic effects on PGE2-induced sterile inflammation, ferroptosis and osteogenesis inhibition. (A) Cell viability of MC3T3-E1 cells after treatment with varying concentrations of Fer-1. (B) Time course of cell viability following 100 ng/mL PGE2 and 10 μ M Fer-1 + 100 ng/mL PGE2 treatment. (C–G): The mRNA expressions of *IL-6*, *Nos2*, *Acsl4*, *Fth1* and *Gpx4*. (H,I): Relative ROS levels assessed by flow cytometry. (J) Relative MDA levels. (K–N) The mRNA expressions of *Runx2*, *Opn*, *Ocn* and *Osterix*. * $P < 0.05$, ** $P < 0.01$, *** $P < 0.001$, **** $P < 0.0001$.

NOS2 knockdown diluted the promoting effect on ferroptosis and the inhibitory effect on osteogenesis of PGE2

NOS2 was knocked down to explore whether NOS2 mediates the regulatory effects of PGE2 on ferroptosis and osteogenesis. NOS2 was confirmed effectively knocked down and its expression level in the inflammatory environment was significantly lower than that in nonknockdown conditions (Fig. 4A–F). The results revealed that at both the genetic and protein levels, NOS2 knockdown attenuated the PGE2-induced significant upregulation of ACSL4 expression and downregulation of FTH1 and GPX4, along with the decreased production of ROS (Fig. 4L,M) and MDA (Fig. 4N). Also NOS2 knockdown upregulated RUNX2 and OPN expression (Fig. 5A–D) impaired by PGE2. Both ALP and ARS staining demonstrated that, after NOS2 knockdown, ALP activity increased (Fig. 5E–G) and Ca^{2+} levels rose (Fig. 5H–J) compared with those treated with PGE2 alone. These effects following NOS2 knockdown showed similar trends to those observed in the Fer-1 treatment group, which showed no statistically significant differences between these groups and the control group.

NOS2 overexpression promoted ferroptosis and inhibited the osteogenesis induced by PGE2

To further validate the mediating role of NOS2, we overexpressed it (Fig. 6A–F) and detected the same indicators. The overexpression of NOS2 further amplified the changes in the expression of ACSL4, FTH1 and GPX4 (Fig. 6G–K), and the relative production levels of ROS (Fig. 6L,M) and MDA (Fig. 6N). The downregulated expression of RUNX2 and OPN induced by PGE2 were significantly further inhibited following NOS2 overexpression (Fig. 7A–D). However, the differences were not statistically significant compared with those in the group treated with PGE2 alone. Similarly, ALP activity (Fig. 7E–G) and mineralized level (Fig. 7H–J), as demonstrated by ALP and ARS staining, showed comparable increases. These differences were statistically significant compared with

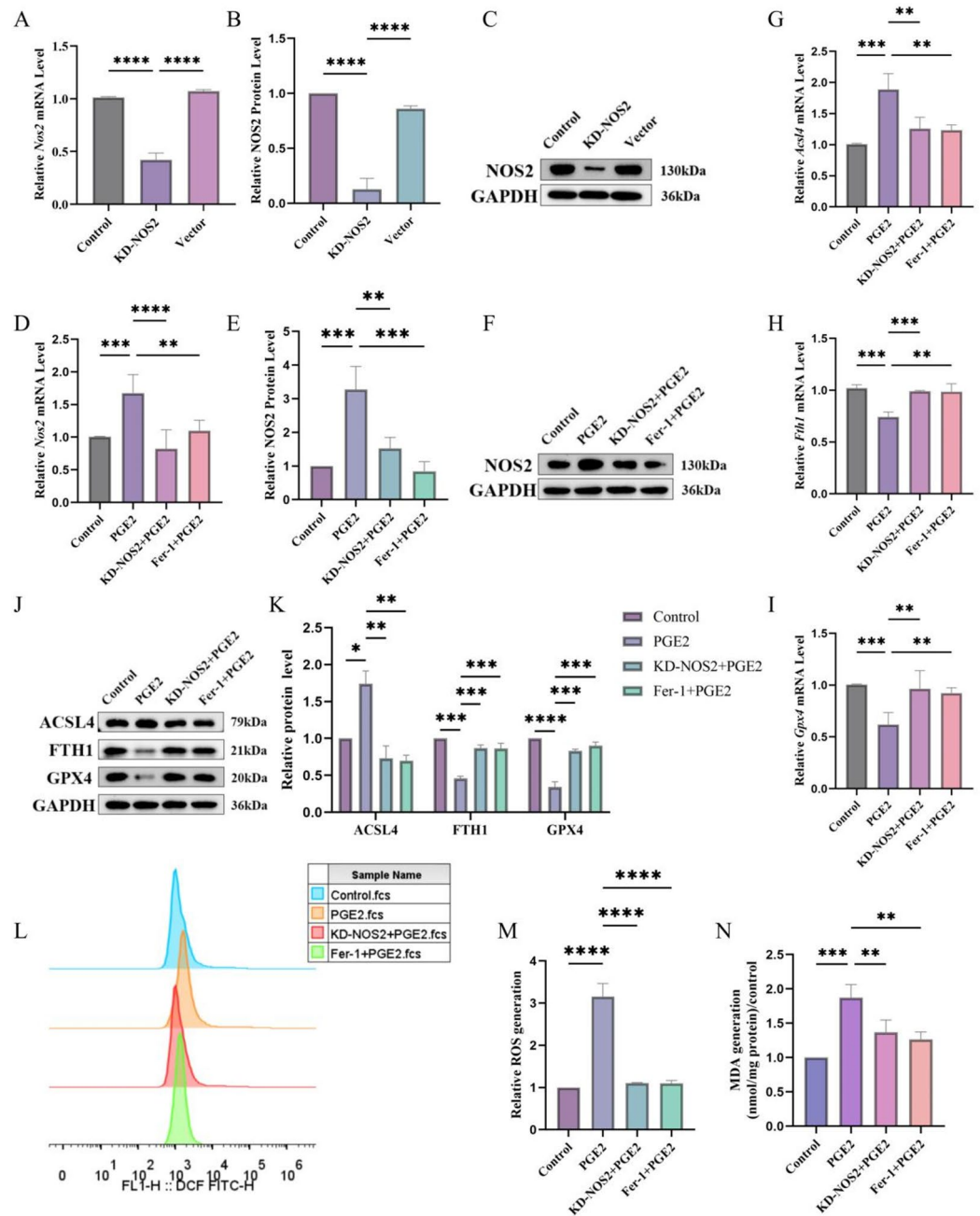


Fig. 4. Effect of NOS2 knockdown on PGE2-induced ferroptosis. (A) The mRNA expressions of *Nos2* after sh-RNA and vector transfection. (B,C) The Western blot results of NOS2 expressions after knockdown. (D) The mRNA expressions of *Nos2* following NOS2 knockdown under sterile inflammatory condition. (E,F) The Western blot results of NOS2 expressions following NOS2 knockdown under sterile inflammatory condition. (G–I) The mRNA expressions of *Acs14*, *Fth1* and *Gpx4*. (J,K) The Western blot results of ACSL4, FTH1 and GPX4 expressions. (L,M) Relative ROS levels assessed by flow cytometry. (Original blots are presented in Supplementary Fig. 1) (N) Relative MDA levels. * $P < 0.05$, ** $P < 0.01$, *** $P < 0.001$, **** $P < 0.0001$.

those in the group treated with PGE2 alone. As a result, at the biochemical level, the enhancing effect of NOS2 overexpression on PGE2 is more pronounced than that at the genetic and protein levels. On the basis of these results, we cautiously concluded that the promoting effect of PGE2 on ferroptosis and the inhibitory effect on osteogenesis in MC3T3-E1 cells could be further enhanced by NOS2 overexpression.

NOS2 overexpression induced ferroptosis and inhibit osteogenesis independent of inflammatory signaling

Results above suggested that PGE2 regulated ferroptosis and osteogenesis in MC3T3-E1 cells by modulating NOS2 expression. To further investigate whether the regulatory capacity of NOS2 depended on inflammatory

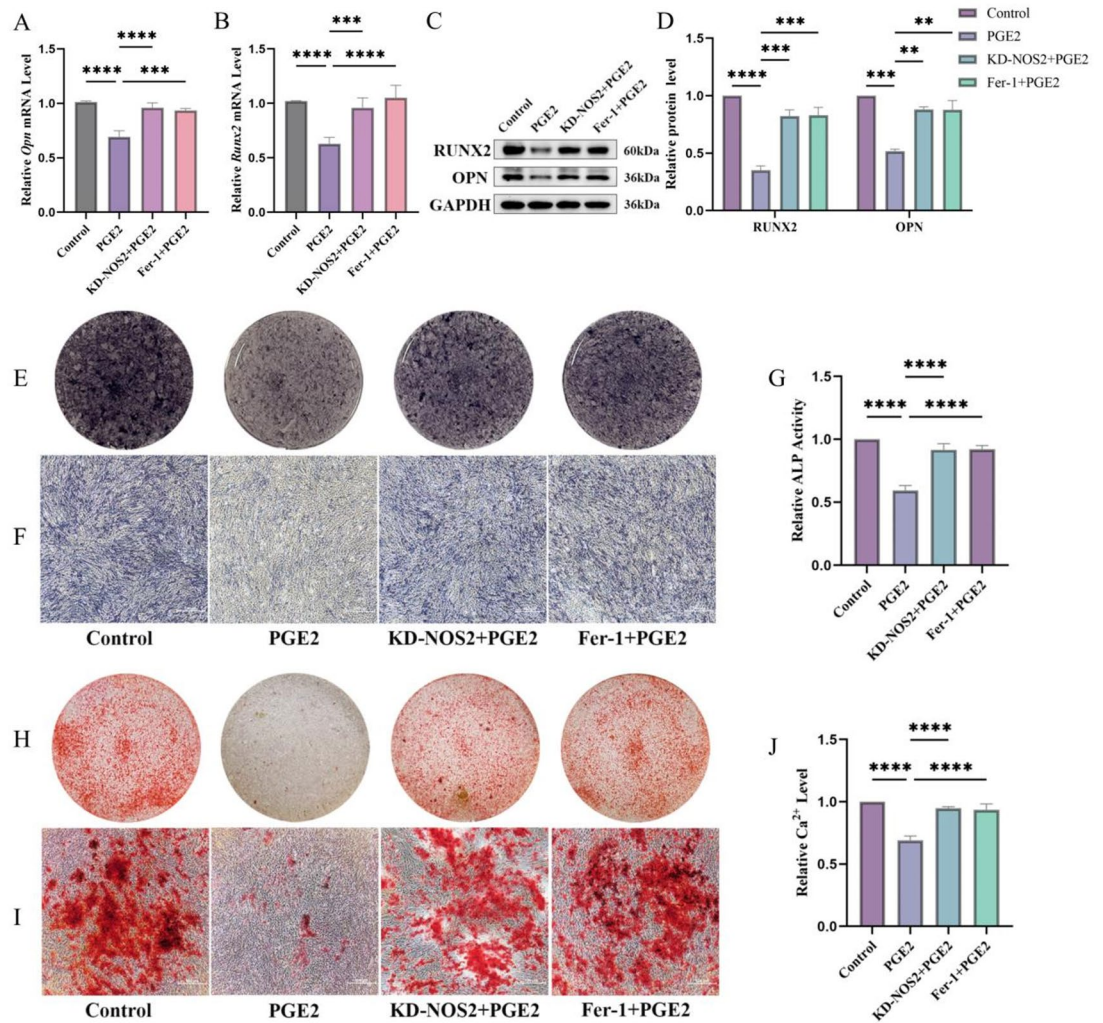


Fig. 5. Effect of NOS2 knockdown on PGE2-inhibited osteogenic activity. (**A,B**): The mRNA expressions of *Runx2* and *Opn*. (**C,D**) The Western blot results of RUNX2 and OPN expressions. (**E,F**) Results of ALP staining (40 \times , bar = 500 μ m, representative images are shown). (**G**) Results of relative ALP activity assay (mean \pm SD, $n = 3$ independent experiments) (**H,I**) Results of ARS staining (40 \times , bar = 500 μ m, representative images are shown). (**J**) Results of relative Ca²⁺ level determination (mean \pm SD, $n = 3$ independent experiments). (Original blots are presented in Supplementary Fig. 2) ** $P < 0.01$, *** $P < 0.001$, **** $P < 0.0001$.

signals, we overexpressed NOS2 under noninflammatory conditions. The results indicated that after NOS2 overexpression, there was a marked promotion of ferroptosis as demonstrated by expression changes of ACSL4, FTH1 and GPX4 at genetic (Fig. 8A–C) and protein levels (Fig. 8D,E), as well as promoted ROS (Fig. 8F,G) and MDA (Fig. 8H) production at biochemical levels. Simultaneously, inhibition of osteogenesis was observed, as evidenced by expression down-regulated of RUNX2 and OPN at mRNA (Fig. 8I,J) and protein levels (Fig. 8K,L), suppressed ALP activity (Fig. 8M–O) and decreased mineralization level (Fig. 8P–R). Interestingly, we unexpectedly discovered an inconsistency in the expression trends of GPX4 at the mRNA and protein levels following NOS2 overexpression, suggesting that under noninflammatory conditions, NOS2 might exert certain complex regulatory effects on GPX4 expression in MC3T3-E1 cells.

Discussion

Orthodontic force application triggers a cascade of molecular events in the periodontal ligament, leading to adaptive remodeling of the alveolar bone. PGE2 is a widely acknowledged pivotal inflammatory mediator involved within this process^{2,20,23}. The MC3T3-E1 cell line, a well-established model for osteogenic differentiation studies, was used in this study. It was demonstrated that 100 ng/mL PGE2 significantly upregulated the expression of the inflammatory cytokines IL-6 and NOS2. Concurrently, ferroptosis-related markers and oxidative products indicated that ferroptosis was induced. These results collectively confirmed a successful establishment of an in vitro model of MC3T3-E1 cells that induced both sterile inflammation and ferroptosis. To assess PGE2-induced inflammation, we initially measured the mRNA levels of IL-1 β and TNF- α . However, the Ct values consistently exceeded 32 cycles, indicating negligible basal and induced expression level in MC3T3-E1 cells.

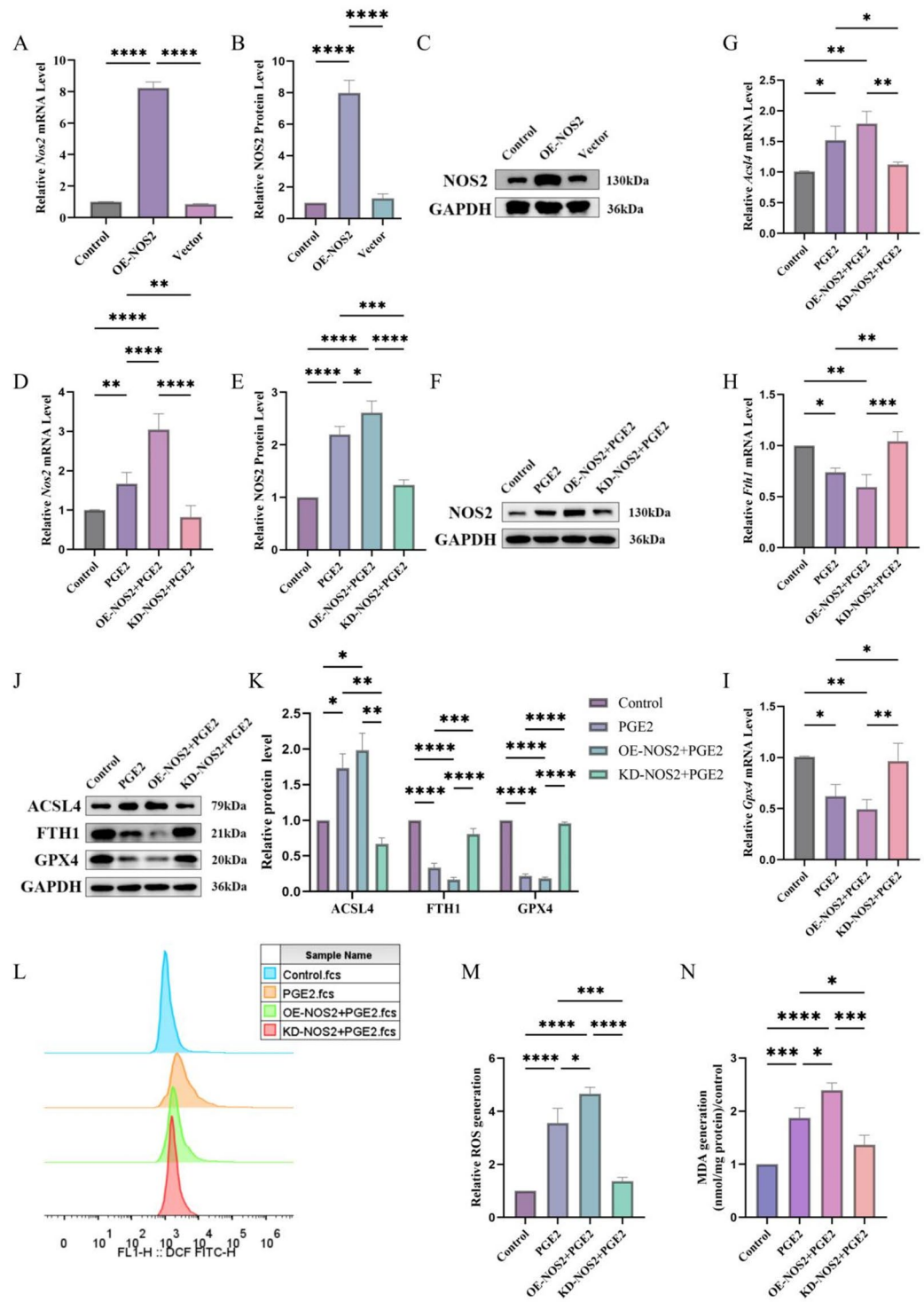


Fig. 6. Effect of NOS2 overexpression on PGE2-induced ferroptosis. (A) The mRNA expressions of *Nos2* after overexpression plasmid and vector transfection. (B,C) The Western blot results of NOS2 expressions after overexpression. (D) The mRNA expressions of *Nos2* following NOS2 overexpression under sterile inflammatory condition. (E,F) The Western blot results of NOS2 expressions following NOS2 overexpression under sterile inflammatory condition. (G–I): The mRNA expressions of *Acsl4*, *Fth1* and *Gpx4*. (J,K) The Western blot results of ACSL4, FTH1 and GPX4 expressions. (L,M) Relative ROS levels assessed by flow cytometry. (Original blots are presented in Supplementary Fig. 3) (N): Relative MDA levels. * $P < 0.05$, ** $P < 0.01$, *** $P < 0.001$, **** $P < 0.0001$.

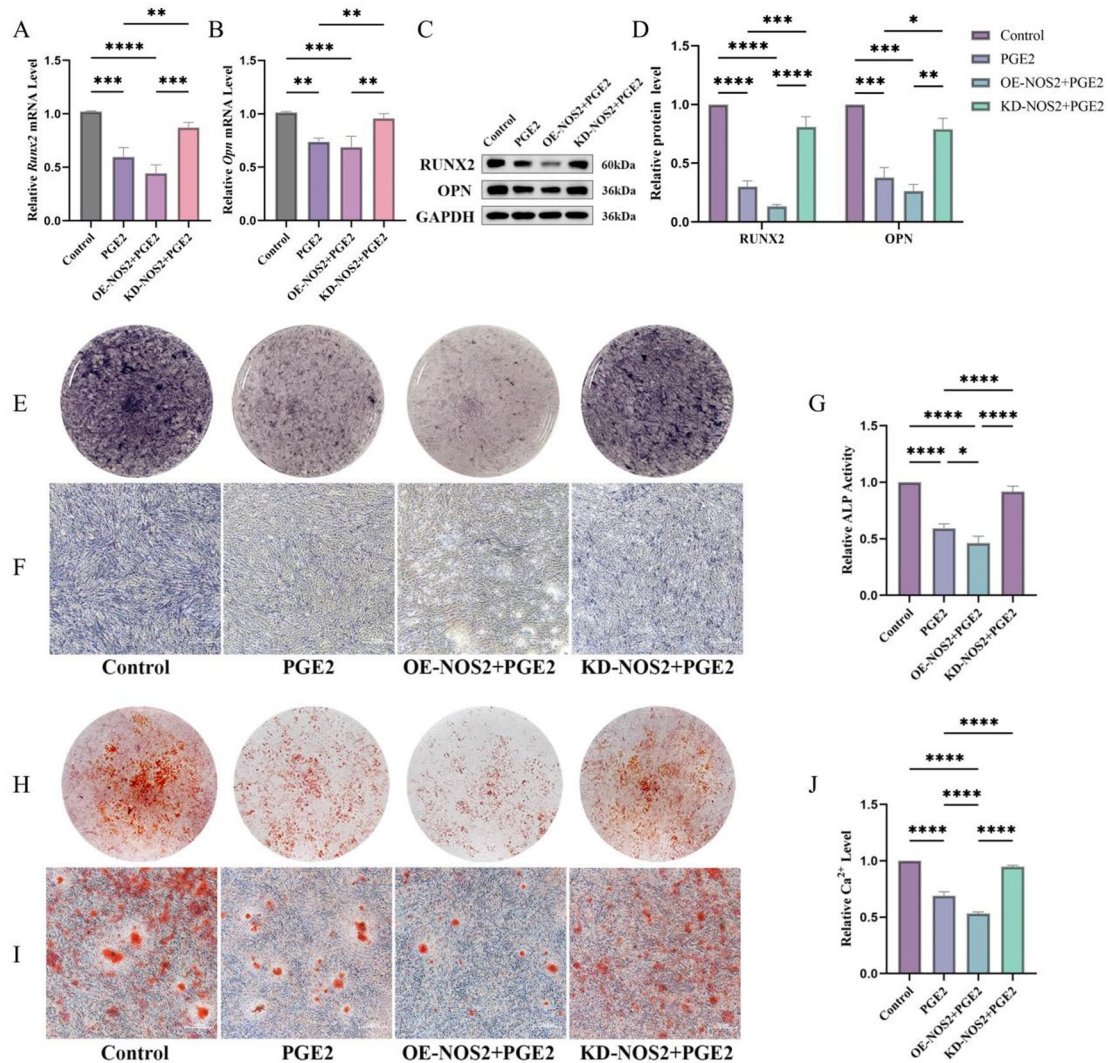


Fig. 7. Effect of NOS2 overexpression on PGE2-inhibited osteogenic activity. (**A,B**) The mRNA expressions of *Runx2* and *Opn*. (**C,D**) The Western blot results of RUNX2 and OPN expressions. (**E,F**) Results of ALP staining (40 \times , bar = 500 μ m, representative images are shown). (**G**) Results of relative ALP activity assay (mean \pm SD, $n = 3$ independent experiments). (**H,I**) Results of ARS staining (40 \times , bar = 500 μ m, representative images are shown). (**J**) Results of relative Ca²⁺ level determination (mean \pm SD, $n = 3$ independent experiments). (Original blots are presented in Supplementary Fig. 4). * $P < 0.05$, ** $P < 0.01$, *** $P < 0.001$, **** $P < 0.0001$.

Due to high variability and low reliability near the quantification limit, these data were excluded. This might suggest cell-type specificity in inflammatory responses. Consistently, prior studies show PGE2 upregulates IL-6 but not TNF- α in MC3T3-E1 cells²⁴, while inhibiting TNF- α but not IL-1 in macrophages²⁵. Furthermore, NOS2 mediates inflammation-induced bone resorption under orthodontic force loading on the compression side²⁶. In the skeletal system, NOS2 serves as a pivotal pro-inflammatory mediator²⁷. Its overexpression has been demonstrated to impair osteogenic function²⁸, induce cellular dysfunction, and disrupt bone metabolic balance²⁹. Meanwhile, IL-6 is a well-established PGE2-responsive inflammatory mediator in osteoblasts^{30–32}. Thus, focusing on IL-6 and NOS2, which showed clear and stable responses in MC3T3-E1 cells, as core inflammatory markers is rational and targeted. The inflammatory characterization focused on IL-6 and NOS2, precluding a comprehensive cytokine profile analysis, is a limitation. Future studies will expand and validate a broader cytokine expression profile.

PGE2 exerts concentration-dependent and context-dependent effects on bone, promoting either formation or resorption^{33–35}. However, the precise mechanisms underlying PGE2-mediated osteogenesis remain incompletely understood. In this study, we observed that PGE2 at a concentration of 100 ng/mL suppressed osteogenesis in MC3T3-E1 cells. This aligns with previous reports of inhibited mineralization by PGE2^{36,37}. Notably, pretreatment with the ferroptosis inhibitor Fer-1 not only attenuated PGE2-induced ferroptosis but also reversed the inhibited osteogenic differentiation. In MC3T3-E1 cells, enhanced ferroptosis is always correlated with diminished osteogenic capacity and vice versa^{38–40}. Our study clarified that PGE2 regulated a synergistic pathological process involving ferroptosis and osteogenic inhibition via NOS2.

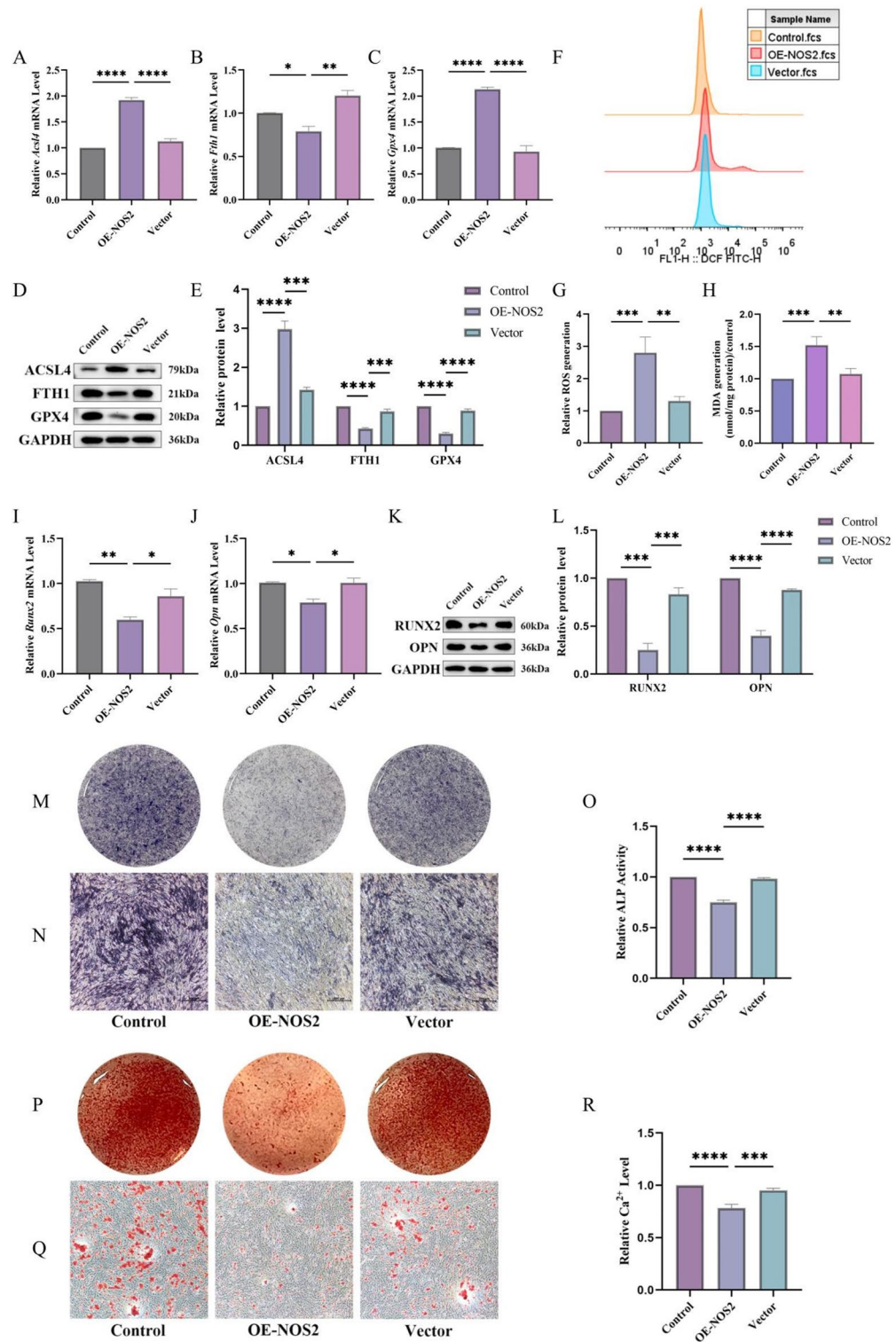


Fig. 8. Effect of NOS2 overexpression in non-inflammation context on ferroptosis and osteogenic function. (A–C) The mRNA expressions of *Acsl4*, *Fth1* and *Gpx4*. (D,E) The Western blot results of ACSL4, FTH1 and GPX4 expressions. (F,G) Relative ROS levels assessed by flow cytometry. (H) Relative MDA levels. (I,J) The mRNA expressions of *Runx2* and *Opn*. (K,L) The Western blot results of RUNX2 and OPN expressions. (M,N) Results of ALP staining (40 \times , bar = 500 μ m, representative images are shown). (O) Results of relative ALP activity assay (mean \pm SD, n = 3 independent experiments). (P,Q) Results of ARS staining (40 \times , bar = 500 μ m, representative images are shown). (R) Results of relative Ca^{2+} level determination (mean \pm SD, n = 3 independent experiments). (Original blots are presented in Supplementary Fig. 5) * P < 0.05, ** P < 0.01, *** P < 0.001, **** P < 0.0001.

NOS2 suppression has been reported to alleviate induced ferroptosis⁴¹, whereas its upregulation exacerbated lipid peroxidation and triggered ferroptosis^{42,43}. However, the regulatory effects of NOS2 on ferroptosis vary across different cell types and conditions, potentially due to cell- and tissue-specific gene expression patterns^{44,45}. As for osteoblast lineage cells, inhibition of NOS2 has been reported to rescue osteogenic differentiation^{28,46}. Our study confirmed that in MC3T3-E1 cells, NOS2 knockdown rescued, while its overexpression potentiated, the PGE2-induced ferroptosis and suppression of osteogenesis. Moreover, NOS2 overexpression alone was sufficient to induce ferroptosis and inhibit osteogenesis. This might be associated with alterations in NO production, which exerts a biphasic effect on osteogenic differentiation, stimulating it at low concentrations and inhibiting it at high concentrations^{47,48}. NO can subsequently activate the cyclooxygenase (COX) pathway, promoting the synthesis of cell-derived PGE2¹⁷. This could partially explain the enhanced PGE2 effects observed following NOS2 overexpression in our study.

An intriguing finding in this study is that following co-treatment with the ferroptosis inhibitor Fer-1 and PGE2, NOS2 expression was upregulated. Combined with the result that NOS2 knockdown alleviates ferroptosis, this suggests a potential bidirectional regulatory loop between them. Existing research evidence provides some clues. On one hand, the ferroptosis inducer RSL3 can drive ferroptosis by promoting NOS dimerization, upregulating NOS2 expression, then increasing NO accumulation⁴⁹. On the other hand, NO, a downstream product of NOS2, has been reported to feedback-regulate its activity and stability through post-translational modifications such as S-nitrosylation⁵⁰. One of the mechanisms of Fer-1 is scavenging lipid peroxides and free radicals^{51,52}, effectively removing ROS/RNS⁵³, and it has been shown to significantly inhibit COX-2 and NOS2 protein expression⁴¹. Since COX-2 catalyzes PGE2 generation⁵⁴, this suggests that inhibiting the “COX-2-PGE2” axis might be one pathway through which Fer-1 reduces NOS2 expression. However, in non-PGE2-induced inflammatory and ferroptosis models in different cell types, Fer-1 has also been observed to downregulate NOS2 expression while inhibiting ferroptosis^{55,56}. Therefore, we speculate that after Fer-1 inhibits ferroptosis, it may feedback-regulate NOS2 expression by altering the intracellular redox homeostasis or specific lipid peroxide signaling. Unfortunately, the specific mechanisms underlying this potential bidirectional loop haven't been reported. It may play a key role in the homeostasis of the bone remodeling microenvironment, providing a new direction for our future research.

Additionally, an intriguing observation was the discordance between molecular expression and functional outcomes following NOS2 overexpression in sterile inflammation environment. While the expression changes in ferroptosis-related genes (GPX4, FTH1, ACSL4) and osteogenic markers (RUNX2, OPN) did not reach statistical significance at the mRNA or protein level, NOS2 overexpression significantly elevated ROS and MDA production and potentially suppressed ALP activity and mineralization. Unfortunately, the mechanistic basis for this discrepancy is yet to be defined. In light of current research, it may be related to the following theories: (1) saturation effect of gene overexpression^{57,58}; (2) negative feedback regulatory mechanisms of gene expression products^{59,60}; (3) inherent constraints on the rate of gene expression due to limited cellular resources and energy⁶¹. The pronounced oxidative stress and lipid peroxidation might arise from intracellular metabolic states and oxidative stress levels being regulated by pathways beyond our experimental scope, such as the GPX4-independent NADPH-FSP1-CoQ10 pathway⁶². Concurrently, NOS2 overexpression leads to a higher level of NO production, the obvious inhibition of osteogenic function is consistent with the documented detrimental effects of sustained high NO levels on osteoblast differentiation^{47,63}.

Research has demonstrated that PGE2 can induce a moderate and controllable acceleration of OTM in animal models while minimizing relapse, compared to corticosteroids and vitamin D, which suggests its potential as a clinical adjunctive therapy⁶⁴. Mechanistically, the NOS/NO system is a central regulator of OTM, with NOS2 primarily mediating inflammation-induced bone resorption on the pressure side^{26,65}. Our study further reveals that PGE2 triggers ferroptosis and impairs osteogenic function via NOS2 activation. Notably, inhibiting ferroptosis has been shown to protect the osteogenic capacity of periodontal ligament stem cells⁶⁶. These suggests that targeting NOS2 could offer a dual benefit: moderately promoting its expression may accelerate OTM, while inhibiting its overactivation can mitigate ferroptosis and preserve bone formation, the latter being the cellular basis for long-term stability. A recent study has confirmed that targeting NOS2/NO effectively promotes OTM⁶⁷, providing a methodological basis. Therefore, elucidating the mechanism of “PGE2-NOS2-Ferroptosis” axis is of significant clinical translational value for developing novel strategies that accelerate OTM while ensuring the quality of bone formation and long-term stability.

Nevertheless, it is prudent to recognize several inherent limitations of this study. First, by knockdown and overexpression, we identified NOS2 as a key mediator, however its downstream signaling events remain incompletely elucidated. Second, it must be noted that this study cannot yet establish whether the observed alteration in osteogenesis is dependent on PGE2-driven ferroptosis. Although we observed that NOS2 knockdown and the established ferroptosis inhibitor Fer-1 produced similar phenotypic rescues, we cannot conclusively attribute the osteogenic effect to ferroptosis mediation. This limitation arises from the potential pleiotropic effects of Fer-1 itself, a study has shown Fer-1 can promote osteogenesis in MC3T3-E1 cells⁶⁸, and our inability to provide definitive evidence through a reverse rescue experiment combining “NOS2 knockdown + ferroptosis inducer”. Therefore, while we can clearly state that PGE2 influences osteogenesis and ferroptosis via NOS2, which suggests a close correlation between NOS2 expression levels and both the ferroptosis process and osteogenic function in MC3T3-E1 cells. But whether the impact of NOS2 on osteogenesis can be attributed to the mediation of ferroptosis requires validation through more precise mechanistic studies in the future. Additionally, The observed discordance between GPX4 mRNA and protein levels following NOS2 overexpression in non-inflammatory context might attribute to buffering mechanisms at the protein level and temporal delays between transcription and translation⁶¹, as well as potentially complex post-transcriptional regulation, which requires further exploration. Finally, this study focused on *in vitro* mechanistic discovery, the mechanistic findings primarily relied on the MC3T3-E1 cells model, which cannot fully recapitulate the complex cellular crosstalk in

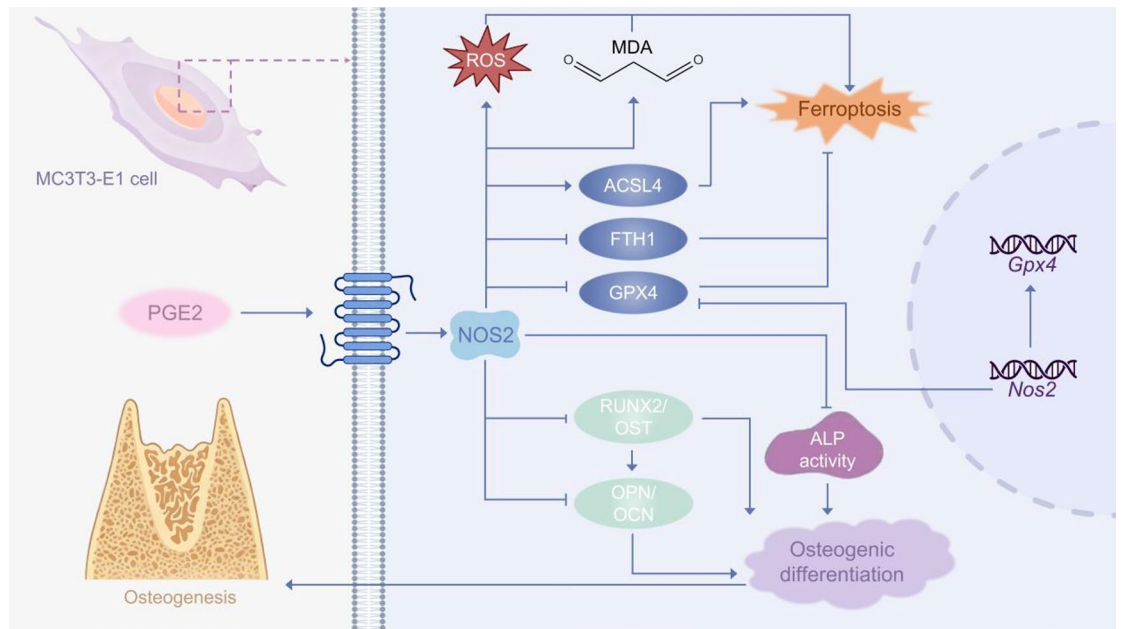


Fig. 9. Experimental research mechanism diagram.

the native periodontal tissue, thereby limiting direct extrapolation to the intact OTM microenvironment. The integrated effects of this pathway in a complex system of relevant animal models await future validation and exploration.

In summary, our findings confirmed the essential impact of NOS2 expression changes in sterile inflammatory and noninflammatory environments in MC3T3-E1 cells, which established NOS2 as a crucial mediator through which PGE2 simultaneously promoted ferroptosis and suppressed osteogenesis, positioning NOS2 as a potential target for modulating bone remodeling.

Conclusion

In this study, we elucidated the critical role of NOS2 mediating the impact of PGE2 on sterile inflammation, ferroptosis and osteogenesis. These findings may pave the way for the theoretical basis of bone remodeling in OTM environment and provide an innovative potential target for accelerating the orthodontic treatment process and maintaining efficacy in future clinical applications (Fig. 9).

Data availability

The datasets used and analysed during the current study are available from the corresponding author on reasonable request.

Received: 2 December 2025; Accepted: 28 February 2026

Published online: 08 March 2026

References

1. Enerbäck, H. et al. Effects of orthodontic treatment and different fluoride regimens on numbers of cariogenic bacteria and caries risk: a randomized controlled trial. *Eur. J. Orthod.* **41**, 59–66. <https://doi.org/10.1093/ejo/cjy025> (2019).
2. Li, Y., Zhan, Q., Bao, M., Yi, J. & Li, Y. Biomechanical and biological responses of periodontium in orthodontic tooth movement: up-date in a new decade. *Int. J. Oral Sci.* **13**, 20. <https://doi.org/10.1038/s41368-021-00125-5> (2021).
3. Steinberg, T., Jung, B., Husari, A., Bai, S. & Tomakidi, P. Shaping Orthodontics of the Future: Concepts and Implications from a Cellular and Molecular Perspective. *Int. J. Mol. Sci.* **26** <https://doi.org/10.3390/ijms26178203> (2025).
4. Wang, L., Wang, C. & He, H. The potential regulatory role of ferroptosis in orthodontically induced inflammatory root resorption. *Int. J. Mol. Sci.* **25** <https://doi.org/10.3390/ijms252413617> (2024).
5. Yamaguchi, M. & Fukasawa, S. Is inflammation a friend or foe for orthodontic treatment? Inflammation in orthodontically induced inflammatory root resorption and accelerating tooth movement. *Int. J. Mol. Sci.* **22** <https://doi.org/10.3390/ijms22052388> (2021).
6. Chen, Y. et al. Integrated bioinformatic analysis of protein landscape in gingival crevicular fluid unveils sequential bioprocess in orthodontic tooth movement. *Prog. Orthod.* **25**, 37. <https://doi.org/10.1186/s40510-024-00536-0> (2024).
7. Shetty, N., Patil, A. K., Ganeshkar, S. V. & Hegde, S. Comparison of ibuprofen and acetaminophen on PGE2 levels in the GCF during orthodontic tooth movement: a human study. *Prog. Orthod.* **14**, 6. <https://doi.org/10.1186/2196-1042-14-6> (2013).
8. Lin, C. et al. Periodontal ligament fibroblasts-derived exosomes induced by PGE(2) inhibit human periodontal ligament stem cells osteogenic differentiation via activating miR-34c-5p/SATB2/ERK. *Exp. Cell. Res.* **419**, 113318. <https://doi.org/10.1016/j.yexcr.2022.113318> (2022).
9. Dixon, S. J. et al. Ferroptosis: an iron-dependent form of nonapoptotic cell death. *Cell* **149**, 1060–1072. <https://doi.org/10.1016/j.cell.2012.03.042> (2012).

10. Jiang, Z. et al. Iron overload-induced ferroptosis of osteoblasts inhibits osteogenesis and promotes osteoporosis: An in vitro and in vivo study. *IUBMB Life*. **74**, 1052–1069. <https://doi.org/10.1002/iub.2656> (2022).
11. Mengjia, W., Jun, J., Xin, Z., Jiahao, Z. & Jie, G. GPX4-mediated bone ferroptosis under mechanical stress decreased bone formation via the YAP-TEAD signalling pathway. *J. Cell. Mol. Med.* **28**, e18231. <https://doi.org/10.1111/jcmm.18231> (2024).
12. Liu, Y. et al. PGE2 pathway mediates oxidative stress-induced ferroptosis in renal tubular epithelial cells. *Febs J.* **290**, 533–549. <https://doi.org/10.1111/febs.16609> (2023).
13. Morotti, M. et al. PGE(2) inhibits TIL expansion by disrupting IL-2 signalling and mitochondrial function. *Nature* **629**, 426–434. <https://doi.org/10.1038/s41586-024-07352-w> (2024).
14. Xu, Y. et al. COX-2/PGE2 pathway inhibits the ferroptosis induced by cerebral ischemia reperfusion. *Mol. Neurobiol.* **59**, 1619–1631. <https://doi.org/10.1007/s12035-021-02706-1> (2022).
15. Marletta, M. A., Yoon, P. S., Iyengar, R., Leaf, C. D. & Wishnok, J. S. Macrophage oxidation of L-arginine to nitrite and nitrate: nitric oxide is an intermediate. *Biochemistry* **27**, 8706–8711. <https://doi.org/10.1021/bi00424a003> (1988).
16. Cooke, J. P. Inflammation and its role in regeneration and repair. *Circ. Res.* **124**, 1166–1168. <https://doi.org/10.1161/circresaha.118.314669> (2019).
17. Kanematsu, M., Ikeda, K. & Yamada, Y. Interaction between nitric oxide synthase and cyclooxygenase pathways in osteoblastic MC3T3-E1 cells. *J. Bone Min. Res.* **12**, 1789–1796. <https://doi.org/10.1359/jbmr.1997.12.11.1789> (1997).
18. Zeng, Q. et al. miR-29b-3p regulated osteoblast differentiation via regulating IGF-1 secretion of mechanically stimulated osteocytes. *Cell. Mol. Biol. Lett.* **24**, 11. <https://doi.org/10.1186/s11658-019-0136-2> (2019).
19. Sun, Y. et al. Force-induced nitric oxide promotes osteogenic activity during orthodontic tooth movement in mice. *Stem Cells Int.* **2022**, 4775445. <https://doi.org/10.1155/2022/4775445> (2022).
20. Choi, Y. T., Kim, Y. J., Yang, K. S. & Lee, D. Y. Bone availability for mandibular molar distalization in adults with mandibular prognathism. *Angle Orthod.* **88**, 52–57. <https://doi.org/10.2319/040617-237.1> (2018).
21. Zhu, L. et al. Self-catalyzed nitric oxide nanocomplexes induce ferroptosis for cancer immunotherapy. *J. Control Release.* **377**, 524–539. <https://doi.org/10.1016/j.jconrel.2024.11.048> (2025).
22. Wang, Z. Y. et al. Targeting inducible nitric oxide synthase with 1400 W mitigates septic acute lung injury through inhibiting SLC7A11/GPX4 mediated ferroptosis. *Nitric Oxide.* **158**, 4–10. <https://doi.org/10.1016/j.niox.2025.05.008> (2025).
23. Jung, J. M., Wi, Y. J., Koo, H. M., Kim, M. J. & Chun, Y. S. Maxillary molar derotation and distalization by using a nickel-titanium wire fabricated on a setup model. *Korean J. Orthod.* **47**, 268–274. <https://doi.org/10.4041/kjod.2017.47.4.268> (2017).
24. Zhang, F. et al. IL-17A stimulates the expression of inflammatory cytokines via celecoxib-blocked prostaglandin in MC3T3-E1 cells. *Arch. Oral Biol.* **55**, 679–688. <https://doi.org/10.1016/j.archoralbio.2010.06.003> (2010).
25. Scales, W. E., Chensue, S. W., Otterness, I. & Kunkel, S. L. Regulation of monokine gene expression: prostaglandin E2 suppresses tumor necrosis factor but not interleukin-1 alpha or beta-mRNA and cell-associated bioactivity. *J. Leukoc. Biol.* **45**, 416–421 (1989).
26. Tan, S. D. et al. Orthodontic force stimulates eNOS and iNOS in rat osteocytes. *J. Dent. Res.* **88**, 255–260. <https://doi.org/10.1177/0022034508330861> (2009).
27. Shen, P. et al. NOS inhibition reverses TLR2-induced chondrocyte dysfunction and attenuates age-related osteoarthritis. *Proc. Natl. Acad. Sci. U S A.* **120**, e2207993120. <https://doi.org/10.1073/pnas.2207993120> (2023).
28. Veeriah, V. et al. Interleukin-1 β , lipocalin 2 and nitric oxide synthase 2 are mechano-responsive mediators of mouse and human endothelial cell-osteoblast crosstalk. *Sci. Rep.* **6**, 29880. <https://doi.org/10.1038/srep29880> (2016).
29. Li, D. et al. METTL3 regulates osteoclast biological behaviors via iNOS/NO-mediated mitochondrial dysfunction in inflammatory conditions. *Int. J. Mol. Sci.* **24** <https://doi.org/10.3390/ijms24021403> (2023).
30. Gruber, R., Nothegger, G., Ho, G. M., Willheim, M. & Peterlik, M. Differential stimulation by PGE(2) and calcemic hormones of IL-6 in stromal/osteoblastic cells. *Biochem. Biophys. Res. Commun.* **270**, 1080–1085. <https://doi.org/10.1006/bbrc.2000.2573> (2000).
31. Kozawa, O., Suzuki, A., Tokuda, H., Kaida, T. & Uematsu, T. Interleukin-6 synthesis induced by prostaglandin E2: cross-talk regulation by protein kinase C. *Bone* **22**, 355–360. [https://doi.org/10.1016/s8756-3282\(97\)00293-7](https://doi.org/10.1016/s8756-3282(97)00293-7) (1998).
32. Murakami, K. et al. A Jak1/2 inhibitor, baricitinib, inhibits osteoclastogenesis by suppressing RANKL expression in osteoblasts in vitro. *PLoS One*. **12**, e0181126. <https://doi.org/10.1371/journal.pone.0181126> (2017).
33. Raisz, L. G. & Fall, P. M. Biphasic effects of prostaglandin E2 on bone formation in cultured fetal rat calvaria: interaction with cortisol. *Endocrinology* **126**, 1654–1659. <https://doi.org/10.1210/endo-126-3-1654> (1990).
34. Tian, X. Y. et al. Continuous infusion of PGE2 is catabolic with a negative bone balance on both cancellous and cortical bone in rats. *J. Musculoskelet. Neuronal Interact.* **7**, 372–381 (2007).
35. Zhang, Y. et al. Tissue regeneration. Inhibition of the prostaglandin-degrading enzyme 15-PGDH potentiates tissue regeneration. *Science* **348**, aaa2340. <https://doi.org/10.1126/science.aaa2340> (2015).
36. Manokawinchoke, J., Pimkhaokhum, A., Everts, V. & Pavasant, P. Prostaglandin E2 inhibits in-vitro mineral deposition by human periodontal ligament cells via modulating the expression of TWIST1 and RUNX2. *J. Periodontal Res.* **49**, 777–784. <https://doi.org/10.1111/jre.12162> (2014).
37. Mirsaidi, A., Tiaden, A. N. & Richards, P. J. Prostaglandin E(2) inhibits matrix mineralization by human bone marrow stromal cell-derived osteoblasts via Epac-dependent cAMP signaling. *Sci. Rep.* **7**, 2243. <https://doi.org/10.1038/s41598-017-02650-y> (2017).
38. Fang, Y. et al. Inhibition of SLC40A1 represses osteoblast formation via inducing iron accumulation and activating the PERK/ATF4/CHOP pathway mediated oxidative stress. *Redox Rep.* **29**, 2428147. <https://doi.org/10.1080/13510002.2024.2428147> (2024).
39. Jiang, Z., Deng, L., Xiang, G., Xu, X. & Wang, Y. A Mechanistic study of the osteogenic effect of arecoline in an osteoporosis model: Inhibition of iron overload-induced osteogenesis by promoting heme oxygenase-1 expression. *Antioxid. (Basel)*. <https://doi.org/10.3390/antiox13040430> (2024).
40. Xu, P. et al. VDR activation attenuates osteoblastic ferroptosis and senescence by stimulating the Nrf2/GPX4 pathway in age-related osteoporosis. *Free Radic. Biol. Med.* **193**, 720–735. <https://doi.org/10.1016/j.freeradbiomed.2022.11.013> (2022).
41. Zhang, W. et al. Canagliflozin attenuates lipotoxicity in cardiomyocytes by inhibiting inflammation and ferroptosis through activating AMPK pathway. *Int. J. Mol. Sci.* **24** <https://doi.org/10.3390/ijms24010858> (2023).
42. Sze, S. C. W. et al. Aberrant transferrin and ferritin upregulation elicits iron accumulation and oxidative inflammation causing ferroptosis and undermines estradiol biosynthesis in aging rat ovaries by upregulating NF-Kb-activated inducible nitric oxide synthase: First demonstration of an intricate mechanism. *Int. J. Mol. Sci.* **23** <https://doi.org/10.3390/ijms232012689> (2022).
43. Wen, Y. et al. Glycyrrhetic acid induces oxidative/nitrative stress and drives ferroptosis through activating NADPH oxidases and iNOS, and depriving glutathione in triple-negative breast cancer cells. *Free Radic. Biol. Med.* **173**, 41–51. <https://doi.org/10.1016/j.freeradbiomed.2021.07.019> (2021).
44. Kapralov, A. A. et al. Redox lipid reprogramming commands susceptibility of macrophages and microglia to ferroptotic death. *Nat. Chem. Biol.* **16**, 278–290. <https://doi.org/10.1038/s41589-019-0462-8> (2020).
45. Qu, W. et al. Targeting iNOS alleviates early brain injury after experimental subarachnoid hemorrhage via promoting ferroptosis of M1 microglia and reducing neuroinflammation. *Mol. Neurobiol.* **59**, 3124–3139. <https://doi.org/10.1007/s12035-022-02788-5> (2022).
46. Duan, S., Zhang, Q., Zhu, J. & Wang, J. SS-31 Targets NOS2 to Enhance Osteogenic Differentiation in Aged BMSCs by Restoring Mitochondrial Function. *Organogenesis* **21**, 2519649. <https://doi.org/10.1080/15476278.2025.2519649> (2025).

47. Mancini, L., Moradi-Bidhendi, N., Becherini, L., Martineti, V. & MacIntyre, I. The biphasic effects of nitric oxide in primary rat osteoblasts are cGMP dependent. *Biochem. Biophys. Res. Commun.* **274**, 477–481. <https://doi.org/10.1006/bbrc.2000.3164> (2000).
48. Tai, Y. T. et al. Pretreatment with low nitric oxide protects osteoblasts from high nitric oxide-induced apoptotic insults through regulation of c-Jun N-terminal kinase/c-Jun-mediated Bcl-2 gene expression and protein translocation. *J. Orthop. Res.* **25**, 625–635. <https://doi.org/10.1002/jor.20365> (2007).
49. Hou, M. J., Huang, X. & Zhu, B. T. Mechanism of RSL3-induced ferroptotic cell death in HT22 cells: crucial role of protein disulfide isomerase. *Acta Biochim. Biophys. Sin. (Shanghai)*. **57**, 616–632. <https://doi.org/10.3724/abbs.2024165> (2024).
50. Foster, M. W. et al. Proteomic analysis of the NOS2 interactome in human airway epithelial cells. *Nitric Oxide*. **34**, 37–46. <https://doi.org/10.1016/j.niox.2013.02.079> (2013).
51. Miotto, G. et al. Insight into the mechanism of ferroptosis inhibition by ferrostatin-1. *Redox Biol.* **28**, 101328. <https://doi.org/10.1016/j.redox.2019.101328> (2020).
52. Skouta, R. et al. Ferrostatins inhibit oxidative lipid damage and cell death in diverse disease models. *J. Am. Chem. Soc.* **136**, 4551–4556. <https://doi.org/10.1021/ja411006a> (2014).
53. Kabiraj, P. et al. The neuroprotective role of ferrostatin-1 under rotenone-induced oxidative stress in dopaminergic neuroblastoma cells. *Protein J.* **34**, 349–358. <https://doi.org/10.1007/s10930-015-9629-7> (2015).
54. Mitchell, J. A., Larkin, S. & Williams, T. J. Cyclooxygenase-2: regulation and relevance in inflammation. *Biochem. Pharmacol.* **50**, 1535–1542. [https://doi.org/10.1016/0006-2952\(95\)00212-x](https://doi.org/10.1016/0006-2952(95)00212-x) (1995).
55. Zhao, J. Y. et al. Injectable thermosensitive hydrogel system based on hyaluronic acid and methylcellulose for the synergistic therapy of traumatic spinal cord injury. *Int. J. Biol. Macromol.* **316**, 144629. <https://doi.org/10.1016/j.ijbiomac.2025.144629> (2025).
56. Wang, X. et al. Astaxanthin attenuates osteoarthritis progression via inhibiting ferroptosis and regulating mitochondrial function in chondrocytes. *Chem. Biol. Interact.* **366**, 110148. <https://doi.org/10.1016/j.cbi.2022.110148> (2022).
57. Rice, A. M. & McLysaght, A. Dosage-sensitive genes in evolution and disease. *BMC Biol.* **15**, 78. <https://doi.org/10.1186/s12915-017-0418-y> (2017).
58. Veitia, R. A. & Potier, M. C. Gene dosage imbalances: action, reaction, and models. *Trends Biochem. Sci.* **40**, 309–317. <https://doi.org/10.1016/j.tibs.2015.03.011> (2015).
59. Bravo-Estupiñan, D. M. et al. Gene dosage compensation: Origins, criteria to identify compensated genes, and mechanisms including sensor loops as an emerging systems-level property in cancer. *Cancer Med.* **12**, 22130–22155. <https://doi.org/10.1002/cam4.6719> (2023).
60. Qiu, C. et al. Stub1 promotes degradation of the activated Diaph3: A negative feedback regulatory mechanism of the actin nucleator. *J. Biol. Chem.* **300**, 107813. <https://doi.org/10.1016/j.jbc.2024.107813> (2024).
61. Liu, Y., Beyer, A. & Aebersold, R. On the Dependency of Cellular Protein Levels on mRNA Abundance. *Cell* **165**, 535–550. <https://doi.org/10.1016/j.cell.2016.03.014> (2016).
62. Ma, T. et al. GPX4-independent ferroptosis—a new strategy in disease's therapy. *Cell. Death Discov.* **8**, 434. <https://doi.org/10.1038/s41420-022-01212-0> (2022).
63. Yang, J. Y. et al. Nitric oxide-induced autophagy in MC3T3-E1 cells is associated with cytoprotection via AMPK activation. *Korean J. Physiol. Pharmacol.* **19**, 507–514. <https://doi.org/10.4196/kjpp.2015.19.6.507> (2015).
64. Hamed, S. A., Mohammad, M. H., Grawish, M. E., Fouda, A. M. & Montasser, M. A. Three pharmacological agents for acceleratory orthodontic tooth movement and subsequent relapse: A randomized controlled animal study. *Int. Orthod.* **24**, 101112. <https://doi.org/10.1016/j.ortho.2025.101112> (2025).
65. Baurmash, H. & DeChiara, S. A conservative approach to the management of orofacial vascular lesions in infants and children: report of cases. *J. Oral Maxillofac. Surg.* **49**, 1222–1225. [https://doi.org/10.1016/0278-2391\(91\)90422-i](https://doi.org/10.1016/0278-2391(91)90422-i) (1991).
66. Lin, C. et al. Klotho protects the osteogenic function of human periodontal ligament stem cells in periodontitis by inhibiting NOX4-mediated ferroptosis. *Stem Cell. Res. Ther.* <https://doi.org/10.1186/s13287-026-04894-w> (2026).
67. Tan, H. et al. Microneedles loaded with nitric-oxide driven nanomotors improve force-induced efferocytosis impairment and sterile inflammation by revitalizing macrophage energy metabolism. *ACS Nano*. **19**, 9390–9411. <https://doi.org/10.1021/acsnano.5c01877> (2025).
68. Valanezhad, A., Odatsu, T., Abe, S. & Watanabe, I. Bone formation ability and cell viability enhancement of MC3T3-E1 cells by ferrostatin-1 a ferroptosis inhibitor of cancer cells. *Int. J. Mol. Sci.* **22** <https://doi.org/10.3390/ijms22212259> (2021).

Author contributions

All the authors have made substantial contributions to the conception and design of the study. M.S. was responsible for the design, experiments execution, data collection and analysis. Y.Y. was responsible for study conception, experiments execution and data analysis. L.P. and J.Y. were in charge of compiling the materials and editing the manuscript. Y.L. collected and analysed the rat OTM model gene expression data. C.L., L.Z. and M.S. interpreted and composed the manuscript. All the authors read and approved the final manuscript.

Funding

This work is funded by the Tianjin Health Research Project [Grand No. TJWJ2024XK019], the Scientific Research Project of Tianjin Education Commission (Natural Science) [Grand No. 2024ZX016], and the Tianjin Natural Science Foundation of China [Grand No. 25]CQJNC01420].

Declarations

Ethics approval and consent to participate

All animal experiments were approved by the Medical Ethics Committee of Tianjin Stomatological Hospital (Approval No.:PA2014-B-016) and were performed in accordance with the institution's guidelines for the care and use of laboratory animals. The authors complied with the ARRIVE guidelines.

Competing interests

The authors declare no competing interests.

Additional information

Supplementary Information The online version contains supplementary material available at <https://doi.org/10.1038/s41598-026-43001-0>.

Correspondence and requests for materials should be addressed to C.L. or L.Z.

Reprints and permissions information is available at www.nature.com/reprints.

Publisher's note Springer Nature remains neutral with regard to jurisdictional claims in published maps and institutional affiliations.

Open Access This article is licensed under a Creative Commons Attribution-NonCommercial-NoDerivatives 4.0 International License, which permits any non-commercial use, sharing, distribution and reproduction in any medium or format, as long as you give appropriate credit to the original author(s) and the source, provide a link to the Creative Commons licence, and indicate if you modified the licensed material. You do not have permission under this licence to share adapted material derived from this article or parts of it. The images or other third party material in this article are included in the article's Creative Commons licence, unless indicated otherwise in a credit line to the material. If material is not included in the article's Creative Commons licence and your intended use is not permitted by statutory regulation or exceeds the permitted use, you will need to obtain permission directly from the copyright holder. To view a copy of this licence, visit <http://creativecommons.org/licenses/by-nc-nd/4.0/>.

© The Author(s) 2026